HYDROTHERMAL SYNTHESIS OF TiO_2/BiOBr COMPOSITES WITH ENHANCED PHOTOCATALYTIC ACTIVITY

by

Kuang WANG[a,b], Zhenming QI[b], Yujie CHEN[a], Jiayi CHEN[b], Yu REN[a], and Chunxia WANG[a,b*]

[a] School of Textile and Clothing, Nangtong University, Jiangsu, China
[b] College of Textiles and Clothing, Yancheng Institute of Technology, Yancheng, China

Original scientific paper
https://doi.org/10.2298/TSCI2203779W

The hydrothermal method is used to fabricate the TiO_2/BiOBr composite. The X-ray diffraction, SEM, X-ray photoelectron spectroscopy, and ultraviolet-visible diffuse reflectance spectroscopy are employed to characterize its crystal structure, physical morphology, chemical composition, and light absorption. Its photocatalytic performance and stability are analyzed by the photocatalytic degradation rate of rhodamine B solution under sunlight irradiation. The composite exhibits the optimal photocatalytic effect when the Ti:Bi molar ratio is 4:1.

Key words: *hydrothermal synthesis, TiO_2, BiOBr, photocatalytic activity*

Introduction

Photocatalytic degradation is considered to be a green, high-efficient and promising strategy in sewage retreatment [1]. There are many photocatalysts, *e.g.*, TiO_2 [2], ZnO [3], and BiOCl [4], which possess great potential in environmental remediation. Among them, TiO_2 has attracted much attention due to its high storage, cost-effectiveness, and non-toxicity. Besides, TiO_2 exhibits many desirable properties, *e.g.*, outstanding chemical, thermal and photocatalytic stability, which make it a good candidate for different applications in coatings, textiles, medical treatment, air purification, and photocatalysis [5]. However, large-scale applications of TiO_2 have been hampered by its wide band gap and recombination of photogenerated carriers. The wide band-gap of TiO_2 (3.0-3.2 eV) may result in the low utilization of sunlight, and recombination of photogenerated carriers may lead to a decrease in photocatalytic quantum efficiency [6].

In recent years, many researchers have devoted to improving the photocatalytic efficiency of TiO_2 through several methods, such as doping with impurities [7], deposition with noble metal [8], sensitization with dye, and combining with other narrow band-gap semiconductors [9, 10]. Among them, combing with other semiconductors, for instance, TiO_2/Ag_3PO_4 [11], TiO_2/g-C_3N_4 [12], TiO_2/WO_3 [13], TiO_2/Bi_2WO_6 [14], TiO_2/Cu_2O [15], and so on, has become a research hotspot recently. As both ultraviolet and visible light-responsive semiconductors, bismuth oxybromide (BiOBr) promises high specific surface area as well as appropriate band position and bandgap [16]. The BiOBr/TiO_2 nanocomposite was prepared by Juntrapirom [17] and his team *via* a thermal hydrolysis process, and the obtained sample can effi-

* Corresponding author, e-mail: cxwang@mail.dhu.edu.cn

ciently synthesis green organics under nature sunlight irradiation. Zhao *et al.* [18] presented a simple co-precipitation method in preparing BiOBr nanosheets@TiO_2 nanobelts photocatalysts, and results revealed that BiOBr@TiO_2 had excellent photocatalytic performance in photocatalytic H_2 production over water splitting and photodegradation of rhodamine B (RhB) under visible light illumination.

Herein, we report the fabrication of hydrangea-like TiO_2/BiOBr photocatalyst by a typical hydrothermal method for sunlight degradation of aqueous RhB. The effect of Ti/Bi molar ratio on photocatalytic activity in RhB degradation was discussed.

Experiments

The TiO_2 was synthesized in our own laboratory in previous work [19]. Bismuth nitrate pentahydrate [$Bi(NO_3)_3 \cdot 5H_2O$, AR] and sodium bromide (NaBr, AR) were purchased from Shanghai Aladdin Bio-Chem Technology Co., Ltd. (Shanghai, China). Anhydrous ethanol (AR), sodium hydroxide (NaOH, AR) and nitric acid (65% HNO_3, AR) were provided by Jiangsu Tongsheng Chemical Reagent Co., Ltd. (Wuxi, China). Rhodamine B (RhB, AR) was obtained from Sinopharm Chemical Reagent Co., Ltd. (Shanghai, China).

The TiO_2/BiOBr samples at various mole ratios of 1:2, 2:1, 4:1, and 6:1 (noted as TB-1, TB-2, TB-4, and TB-6) were synthesized by a facile hydrothermal method. The mole ratio of Bi/Br was 2:3. In a typical procedure, a stoichiometric amount of NaBr was added in 30 mL deionized water under continuous magnetic stirring to obtain a transparent solution A. Meanwhile, an appropriate amount of TiO_2 and $Bi(NO_3)_3 \cdot 5H_2O$ were added in 40 mL HNO_3 solution (1.44 M) with ultrasonic dispersion for 30 minutes to form white suspension B. After that, solution A was dropped into suspension B under stirring, and the pH value of the resulting suspension was adjusted to 7.0 by adding aqueous NaOH. After stirring for another 30 minutes, the suspension was poured into a 100 mL teflon-lined autoclave and heated at 160 ℃ for 12 hours. After being air-cooled to room temperature, the precipitates were separated centrifugally and washed three times with deionized water and anhydrous ethanol, respectively. Finally, the samples were oven-dried at 60 ℃ for 8 hours. Pure BiOBr was prepared in the same method without the presence of TiO_2.

The crystal structure of the obtained sample was identified *via* X-ray diffraction (XRD, PANalytical, Dutch). The surface morphology of the sample was investigated by Nova Nano SEM 450 field emission scanning electron microscope (FESEM, FEI, America). The surface chemical composition was revealed using ESCALAB 250Xi X-ray photoelectron spectrometer model (XPS, Thermo Fisher Scientific, America). The optical absorption spectrum of the sample was taken on TU-1901 UV-visible spectrophotometer (UV-vis DRS, Persee, China) using $BaSO_4$ as reference.

Photocatalytic activities of the obtained samples were evaluated by degradation of 15 mg/L RhB solution under sunlight (300 W Xe lamp, LS-SXE300/300UV). Typically, 0.1 g photocatalysts were scattered into 100 mL RhB solution. Before illumination, the resulting suspension was magnetically stirred for 30 minutes in the dark to establish the adsorption-desorption equilibrium between the photocatalysts and RhB. After that, the suspension was exposed to light irradiation under magnetic stirring. At given time intervals, 3 mL suspension was sampled at 10 minutes interval and centrifuged to remove the photocatalysts. The absorbance of RhB solution was recorded by the maximum absorption band at λ = 554 nm on a UV-vis spectrophotometer. The photocatalytic activity of the sample was determined by degradation rate, which was calculated by the formula $DR = 1 - C_t/C_o$, where C_o is the initial concentration of RhB and C_t is the concentration of RhB solution at different irradiation times [20].

Experimental results

The crystal structures of TiO_2, BiOBr, TB-1, TB-2, TB-4, and TB-6 are studied by XRD patterns. As illustrated in fig. 1(a), the characteristic peaks at 20 of 25.28°, 36.98°, 37.93°, 48.34°, 53.99°, 54.93°, 62.69°, 68.83°, 70.09°, and 75.02° belonged to the (101), (103), (004), (200), (105), (211), (204), (113), (220), and (215) crystalline planes of anatase TiO_2 (JCPDS no. 21-1272), respectively. The characteristic peaks at 20 of 27.32°, 36.09°, 41.22°, 44.14°, 54.36°, and 56.45° corresponded to the (110), (101), (111), (210), (211), and (220) planes of rutile TiO_2 (JCPDS no. 21-1276), separately [19]. The diffraction peaks locating at round 10.90°, 21.92°, 31.70°, 32.22°, 33.17°, 34.13°, 39.30°, 44.70°, 46.22°, 50.65°, 53.36°, 56.14°, 57.13°, 66.25°, 67.44°, 70.95°, 76.45°, 76.72°, and 78.70° matched well with (001), (002), (102), (110), (003), (111), (112), (004), (200), (104), (211), (114), (212), (204), (220), (214), (302), (310), and (116) planes of BiOBr (JCPDS no. 78-0348) [21]. All this suggested that TiO_2 and BiOBr were successfully coupled to obtain TiO_2/BiOBr photocatalyst.

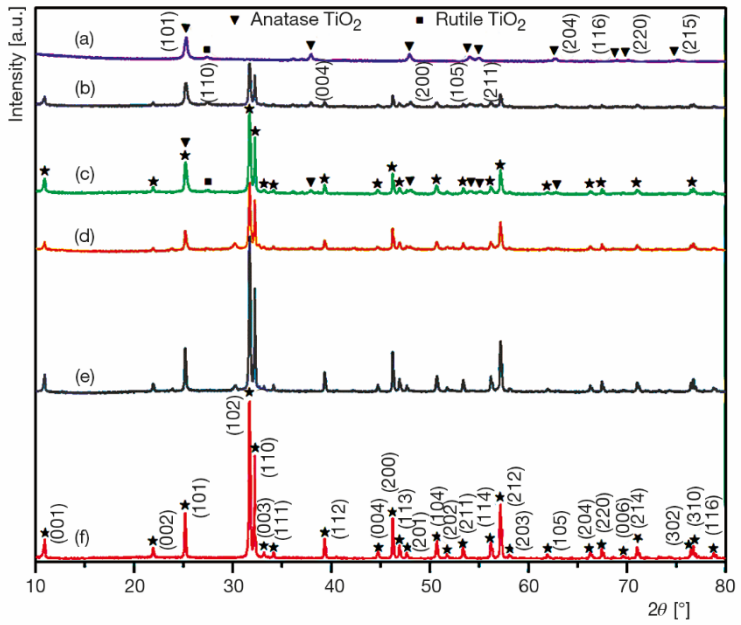

Figure 1. The XRD patterns of (a) TiO_2, (b) TB-6, (c) TB-4, (d) TB-2, (e) TB-1, and (f) BiOBr

In order to observe the distinctive morphology of TB-4, SEM micrographs were taken, as shown in fig. 2. The prepared TB-4 displayed hydrangea shapes with a diameter of about 3~6 μm. In addition, it was noted that the sample is composed of TiO_2 nanorods and BiOBr nanosheets. Among them, the BiOBr nanosheet was estimated to be about 50~130 nm in thickness. The TB-4 had a rough surface, which was beneficial for dye adsorption as well as light absorption and reflection. Thus, the photocatalytic effect was improved.

To shed light on the specific chemical states of TB-4 and the peak fitting of each element, XPS measurement is performed. As the survey spectrum showed in fig. 3(a), Ti, O, Bi, and Br were detected in TB-4. What was worth mention, the peak at 284.8 eV was attributed to

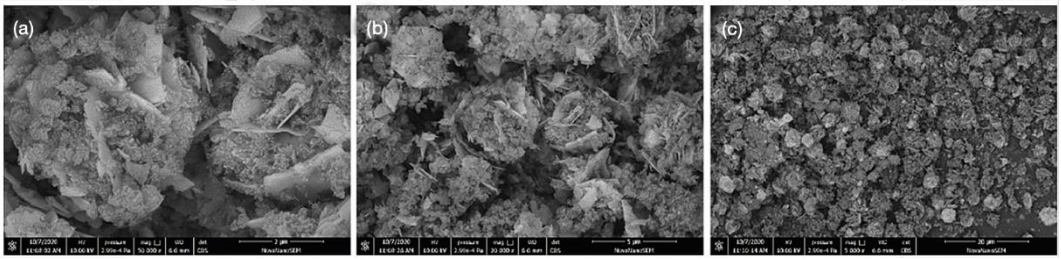

Figure 2. The SEM micrographs of TB-4: (a) ×50000, (b) ×20000, and (c) ×5000

the characteristic peak of C 1 second, which was brought by oil contamination during the measurement. In fig. 3(b), two peaks at 164.5 eV and 159.2 eV in Bi 4f spectrum can be ascribed to Bi $4f_{5/2}$ and Bi $4f_{7/2}$, indicating the existence of Bi^{3+} in TiO_2/BiOBr [21]. In fig. 3(c), the peaks at 464.5 eV and 458.7 eV in Ti 2p spectrum were consistent with Ti $2p_{1/2}$ and Ti $2p_{3/2}$, respectively, with an interval of 5.7 eV between the two peaks, which implied the existence of Ti^{+4} [19]. Partial overlaps between characteristic peaks of Ti $2p_{1/2}$ at 464.5 eV and Bi $4d_{3/2}$ at 467.1 eV resulted in a broad bump of Ti $2p_{1/2}$ [18]. In fig. 3(d), the peaks at 59.5 eV and 68.4 eV in Br 3d spectrum corresponded to Br $3d_{3/2}$ and $Br3d_{5/2}$, respectively, indicating the presence of Br^{-1} in TiO_2/BiOBr [21]. Figure 3(e) showed the O 1 second spectrum with the characteristic peaks at 529.7 eV, 530.4 eV, and 532.2 eV, which may be assigned to the binding energy of Bi-O, Ti-O, and H-O, respectively [18]. XPS analysis proved that TiO_2 was successfully coupled with BiOBr.

The optical absorption performance of the prepared samples is performed *via* UV-vis DRS, as illustrated in fig. 4. And the band gap of the as-prepared sample is evaluated by eq. (1). As was shown, the absorption edges of TiO_2, TB-4, and BiOBr were at 404 nm, 418 nm, and 447 nm, respectively, and the corresponding band-gaps were 3.07 eV, 2.95 eV, and 2.77 eV, respectively.

$$\alpha h\nu = A(h\nu - Eg)^{\frac{n}{2}} \tag{1}$$

where α is the absorption coefficient, h – the Planck's constant, ν – the frequency, A – the proportional constant of the semiconductor catalyst, and Eg – the band gap [22]. Besides, n depends on the interband transition type of the semiconductor catalyst, and n is taken as 2 for direct transition and 4 for indirect transition [23]. Herein, n is taken as 4 for both TiO_2 and BiOBr, which are indirect transitional semiconductor photocatalysts. Thereafter, $h\nu \sim (ah\nu)^{1/2}$ is obtained, and the band gap can be obtained.

The photodegradation curves of RhB solution by the prepared samples under sunlight irradiation are illustrated in fig. 5(a). It was obvious that the RhB solution was completely photodegraded by all the samples within 60 minutes. Among them, TB-4 had the best photodegradation rate, which can completely degrade RhB within 30 minutes. The photodegradation of RhB solution is verified by pseudo-first-order kinetic curves in fig. 5(b). The constant, K, of TB-4 was about 0.09773 per minute, which ranked first among all the samples. Two possible reasons might lead to this, one was the rough surface, and the other one was the formation of heterojunction structures. The rough surface could adsorb more dye molecules, and the heterojunction structures could inhibit carrier recombination, resulting in enhanced photocatalytic activity.

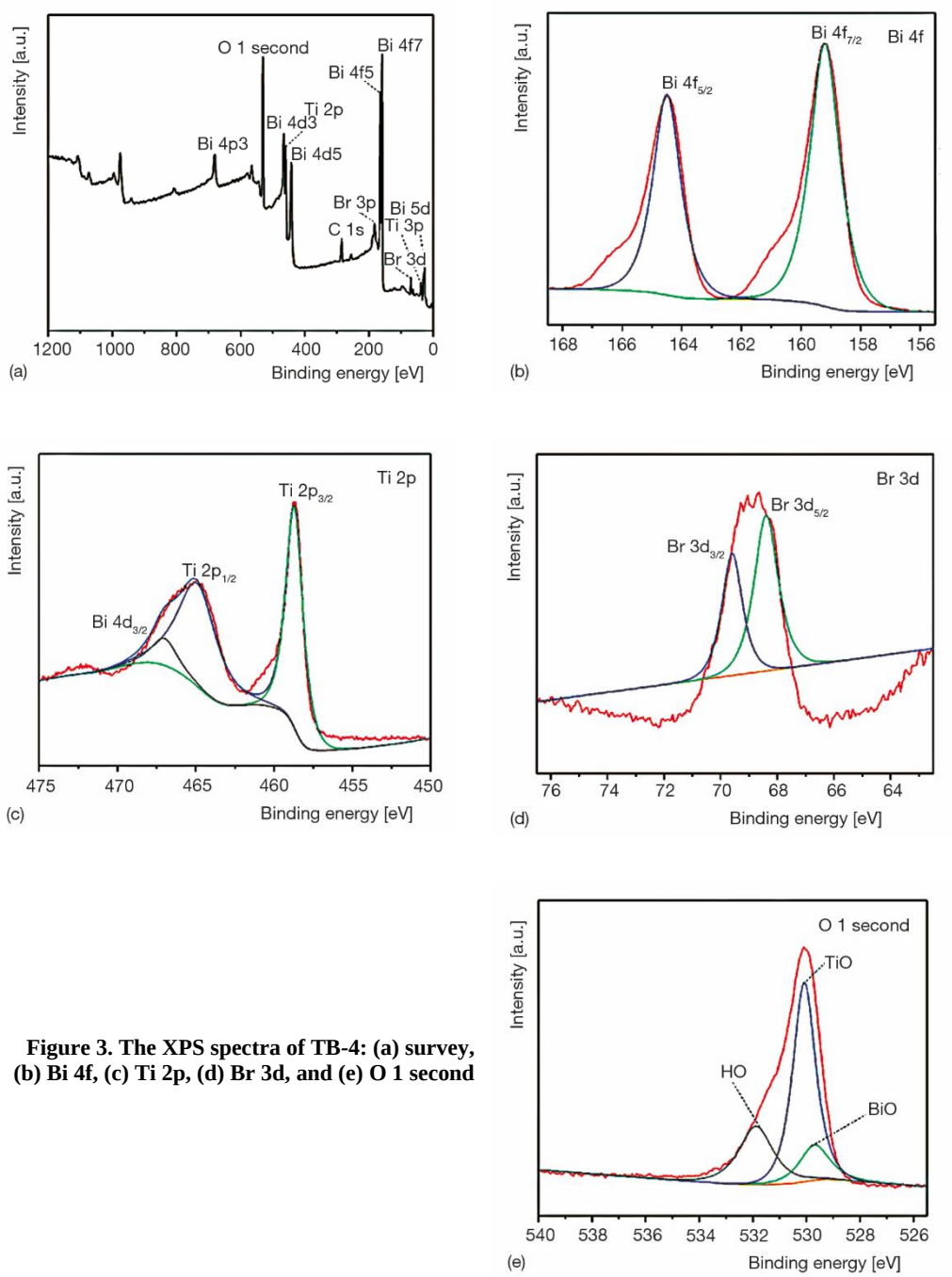

Figure 3. The XPS spectra of TB-4: (a) survey, (b) Bi 4f, (c) Ti 2p, (d) Br 3d, and (e) O 1 second

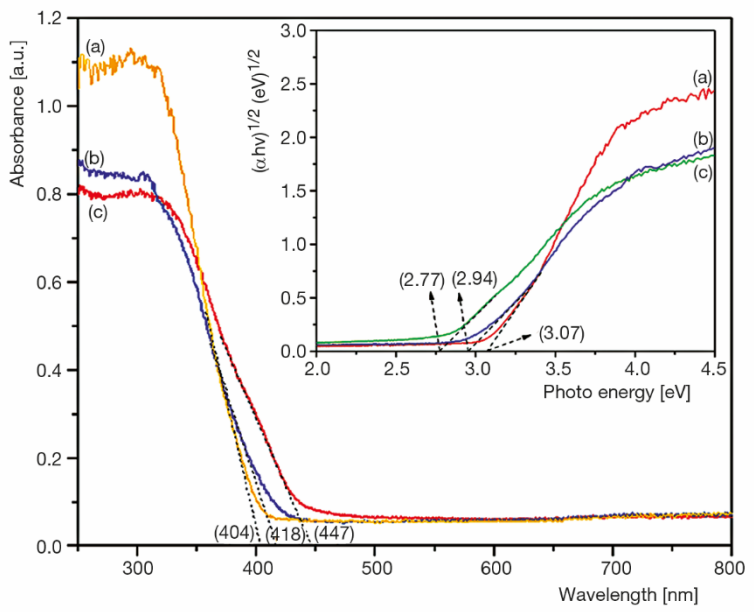

Figure 4. The UV-vis DRS and the corresponding energy gaps (inset): (a) TiO_2, (b) TB-4, and (c) BiOBr

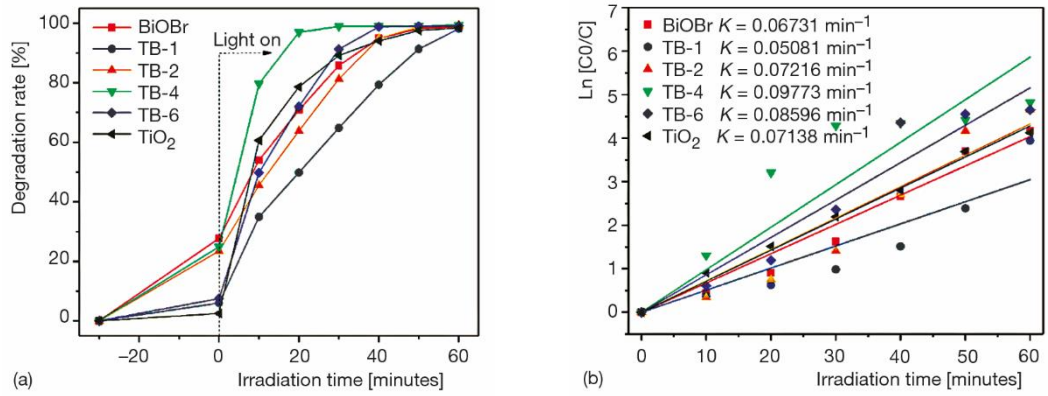

Figure 5. Photocatalytic degradation rates of RhB solution by different photocatalysts at various sunlight irradiation times; (a) photocatalytic degradation and (b) photocatalytic pseudo-first-order kinetic

Discussion and conclusions

In this paper, a facile hydrothermal method was employed to synthesize TiO_2/BiOBr photocatalyst with the growth of BiOBr nanosheets on the surface of TiO_2 nanorods. The as-prepared TiO_2/BiOBr was systematically investigated by XRD, SEM, XPS, and UV-vis DRS analysis. When the mole ratio of Ti:Bi was 4:1, the prepared TiO_2/BiOBr showed a hydrangea-like structure with a rough surface and had the optimal photocatalytic activity under sunlight irradiation, and a strict optimization design for fabrication of the composite is needed using the optimization theory. These new findings prove that the combination of TiO_2 and BiOCl is a commendable strategy for water purification.

References

[1] Khaki, M. R. D., *et al.*, Application of Doped Photocatalysts for Organic Pollutant Degradation-A Review, *Journal of Environmental Management Part 2*, *198* (2017), Aug., pp. 78-94
[2] Pelaez, M., *et al.*, A Review on the Visible Light Active Ttitanium Dioxide Photocatalysts for Environmental Applications, *Applied Catalysis B-Environmental*, *125* (2012), Aug., pp. 331-349
[3] Lam, S. M., *et al.*, Degradation of Wastewaters Containing Organic Dyes Photocatalysed by Zinc Oxide: a Review, *Desalination and Water Treatment*, *41* (2012), 1-3, pp. 131-169
[4] Wang, J., *et al.*, Co-Precipitation Synthesis and Photocatalytic Properties of BiOCl Microflowers, *Optik*, *204* (2020), Feb., 164149
[5] Schneider, J., *et al.*, Understanding TiO_2 Photocatalysis: Mechanisms and Materials, *Chemical Reviews*, *114* (2014), 19, pp. 9919-9986
[6] Cai, C. J., *et al.*, A Green and Facile Route for Constructing Flower-shaped TiO_2 Nanocrystals Assembled on Graphene Oxide Sheets for Enhanced Photocatalytic Activity, *Nanotechnology*, *24* (2013), 27, . 275602
[7] Wang, Y., *et al.*, First-Principles Study of the Electronic Structure of Nonmetal-doped Anatase TiO_2. *Journal of the Korean Physical Society*, *68* (2016), 3, pp. 409-414
[8] Pei, Z., *et al.*, Defect Self-doped TiO_2 for Visible Light Activity and Direct Noble Metal Anchoring. *Physical Chemistry Chemical Physics*, *16* (2014), 39, pp. 21876-21881
[9] Pan, L., *et al.*, Water-Mediated Promotion of Dye Sensitization of TiO_2 under Visible Light, *Journal of the American Chemical Society*, *133* (2011), 26, pp. 10000-10002
[10] Shao, M., *et al.*, TiO_2 Nanotube-Based Composites: Synthesis and Applications, *Science of Advanced Materials*, *5* (2013), 8, pp. 962-981
[11] Jia, Y., *et al.*, Efficient Visible-Light-Responsive Photocatalyst: Hybrid TiO_2-Ag_3PO_4 Nanorods, *Chemical Physics*, *521* (2019), May, pp. 1-4
[12] Zhao, S., *et al.*, g-C_3N_4/TiO_2 Hybrid Photocatalyst with Wide Absorption Wavelength Range and Effective Photogenerated Charge Separation, *Separation and Purification Technology*, *99* (2012), Oct., pp. 50-54
[13] Yang, J., *et al.*, Heterostructured TiO_2/WO_3 Porous Microspheres: Preparation, Characterization and Photocatalytic Properties, *Catalysis Today*, *201* (2013), Mar., pp. 195-202
[14] Hou, Y. F., *et al.*, Facile Hydrothermal Synthesis of TiO_2-Bi_2WO_6 Hollow Superstructures with Excellent Photocatalysis and Recycle Properties, *Dalton Transactions*, *43* (2014), 3, pp. 1025-1031
[15] Shifu, C., *et al.*, Study on the Photocatalytic Activity of p-n Junction Photocatalyst Cu_2O/TiO_2, *Journal of Nanoscience and Nanotechnology*, *9* (2009), 7, pp. 4397-4403
[16] Yang, Y., *et al.*, BiOX (X = Cl, Br, I) Photocatalytic Nanomaterials: Applications for Fuels and Environmental Management, *Advances in Colloid and Interface Science*, *254* (2018), Apr., pp. 76-93
[17] Juntrapirom, S., *et al.*, Natural Sunlight Driven Photocatalytic Coupling of Primary Amines over TiO_2/BiOBr Heterojunction, *Applied Surface Science*, *545* (2021), Apr., 149015
[18] Zhao, Y., *et al.*, Fabrication of BiOBr Nanosheets@TiO_2 Nanobelts p-n Junction Photocatalysts for Enhanced Visible-light Activity, *Applied Surface Science*, *365* (2016), Mar., pp. 209-217
[19] Wang, K., *et al.*, Crystalline Phase Regulation of Anatase-rutile TiO_2 for the Enhancement of Photocatalytic Activity, *RSC Advances*, *10* (2020), 71, pp. 43592-43598
[20] Wang, C. X., *et al.*, $Ag_6Si_2O_7$/CNTs with Highly Efficient and Stable Visible Light Photocatalytic Activity, *Integrated Ferroelectrics*, *198* (2019), 1, pp. 73-79
[21] Lu, L., *et al.*, Tuning the Physicochemical Property of BiOBr *via* pH Adjustment: Towards an Efficient Photocatalyst for Degradation of Bisphenol A, *Journal of Molecular Catalysis A-Chemical*, *423* (2016), Nov., wpp. 379-385
[22] Butler, M. A., Photoelectrolysis and Physical Properties of the Semiconducting Electrode WO_2, *Journal of Applied Physics*, *48* (1977), 5, pp. 1914-1920
[23] Zhang, K., *et al.*, Study of the Electronic Structure and Photocatalytic Activity of the BiOCl Photocatalyst, *Applied Catalysis B-Environmental*, *68*, (2006), 3-4, pp. 125-129

Paper submitted: May 16, 2020
Paper revised: May 10, 2021
Paper accepted: May 16, 2021